Ann. Geophysicae 16, 931–939 (1998) © EGS – Springer-Verlag 1998

Annales Geophysicae

Hydrogen and helium isotope inner radiation belts in the Earth's magnetosphere

G. I. Pugacheva[1], **W. N. Spjeldvik**[2], **A. A. Gusev**[1], **I. M. Martin**[1], **and N. M. Sobolevsky**[3]

[1] University of Campinas, Instituto de Fisica/DRCC, 13083-970, Campinas, SP, Brazil
[2] Department of Physics, Weber State University, Ogden, Utah, 84408-2508, USA
[3] Institute of Nuclear Research of Russian Academy of Science, 117312, Moscow, Russia

Received: 24 July 1997 / Revised: 6 February 1998 / Accepted 16 March 1998

Abstract. Radial transport theory for inner radiation zone MeV ions has been extended by combining radial diffusive transport and losses due to Coulomb friction with local generation of D, T and ^{3}He ions from nuclear reactions taking place on the inner edge of the inner radiation zone. Based on interactions between high energy trapped protons and upper atmospheric constituents we have included a nuclear reaction yield D, T and ^{3}He flux source that was numerically derived from a nuclear reaction model code originally developed at the Institute of Nuclear Researches in Moscow, Russia. Magnetospheric transport computations have been made covering the L-shell range $L = 1.0$–1.6. The resulting MeV energy D, T and ^{3}He ion flux distributions show a strong influence of the local nuclear source mechanism on the inner zone energetic D, T and ^{3}He ion content.

Key words: Atmospheric composition and structure (Thermosphere-composition and chemistry) · Magnetospheric physics (Energetic particles, trapped).

Introduction

Launch of the NASA SAMPEX spacecraft and the complement of Earth orbiting spacecraft in the ISTP/GGS Program have given new impetus to the study of the inner radiation zone of the Earth. Trapping of anomalous cosmic rays (ACR) forming an inner radiation belt of preferentially heavier ions such as atomic oxygen ions and heavier ion species (e.g. Cummings *et al.*, 1994; Selesnick *et al.,* 1995; and references therein) and decay of cosmic ray albedo neutrons (CRAND) are important sources of trapped radiation. But there are also internal sources of ions heavier than protons within the Earth's radiation belts. These include nuclear reactions between geomagnetically confined corpuscular radiation and the heavier neutral species of the Earth's upper atmosphere. In this work we explicitly demonstrate that such processes can generate appreciable trapped fluxes of hydrogen and helium isotope ions and we evaluate the contribution of this internal nuclear hydrogen and helium isotope ion source in the simultaneous context of radially driven sources of energetic hydrogen and helium isotope ion. Nuclear interactions between inner zone protons and atoms of upper atmosphere as a source of energetic deuterium, ^{3}He, and ^{4}He for the ion radiation belt were recently considered by the SAMPEX (Selesnick and Mewaldt, 1996) and CRRES (Chen *et al.*, 1996) research groups. To calculate the intensity of deuterium and helium isotope ions Selesnick and Mewaldt, (1996) and Chen *et al.*, (1996) used a continuity equation accounting for atmospheric production of particles in nuclear reactions and ionization energy losses in the atmosphere. But the ion lifetime due to Coulomb energy losses increases with increasing L-shell due to atmospheric density deceasing. And, in contrast, ion lifetime versus radial transport decreases with increasing L-shell. As a result, the radial diffusion process begins to dominate the ion dynamics at the higher L-shells. Thus, to compute the theoretically expected distribution of isotopes in the radiation belts, it is appropriate to combine the source rates of isotope production with the full transport and loss theory for the inner radiation zone.

The terrestrial exosphere and inner zone energetic proton fluxes

It is possible to generate energetic deuterium, tritium and ^{3}He ions in local nuclear interactions in a narrow altitude range where there is an optimum combination of ambient multi-MeV protons (as collisional projec-

Correspondence to: G. Pugacheva
E-mail: GALINA@IFI.UNICAMP.BR

tiles) and sufficient abundance of the heavier exospheric thermal neutral particle species, such as helium and atomic oxygen and nitrogen. In this work, we consider the generation of energetic isotope ions by the collisional action of trapped protons with energies in the range of 20–1000 MeV at the equatorial crossing of the geomagnetic field lines at $L = 1.1$–2.0 impinging on atomic oxygen and helium. For a reasonable description of the trapped proton fluxes we used the NASA AP-8 model (Vette, 1991), corresponding to solar minimum conditions where the proton fluxes in this region are highest. We recognize that the AP-8 model has its imperfections, and our results are scalable as updated main radiation belt models become available. The chemical composition and number density of the upper atmospheric constituents were taken from the Earth's atmosphere model MSIS-86 (Hedin, 1987). Because of seasonal asymmetries in the exosphere, we averaged the MSIS-86 atmospheric helium and oxygen densities over local time, days of year, (taking the values of the solar index $F10.7 = 140$ and the geophysical index $Ap = 4$) along the drift trajectories of 10, 100 and 1000 MeV protons moving as governed by Lorentz equation at fixed L-shell with equatorial pitch-angle of 90° in the IGRF95 geomagnetic field (Fig. 1)

Using data of drift averaged atmospheric densities ρ (Fig. 1) we computed the 10, 100 and 1000 MeV helium ion lifetime (Fig. 2) due to Coulomb energy losses at the equatorial top of the geomagnetic lines taking into account that $\tau = E/(\rho v)\mathrm{d}E/\mathrm{d}x = E/\mathrm{d}E/\mathrm{d}t$ (Schulz and Lanzerotti, 1974), where E and v represent ion kinetic energy and ion velocity respectively. The $\mathrm{d}E/\mathrm{d}x$ data for helium ion energy losses in units of energy/g $\cdot$ cm^{-2} were extracted from Hubert *et al.* (1990). To estimate the effective ion transport lifetimes due to radial diffusion transport, we used the expression for magnetic radial diffusion $1/\tau = 160 \cdot Do \cdot L^8$, 1/s (Tverskoy, 1968) since magnetic fluctuation radial transport dominates over electric field effects in the upper MeV energy range. In Fig. 2 one can see that the radial diffusion lifetimes are shorter than the Coulomb loss lifetimes for high energy ions in the MeV range at $L > 1.25$–1.3. For empirical comparisons there exist radiation belt observations by the CRRES spacecraft (detector energy range at hundreds of MeV and above), and the SAMPEX spacecraft (instrumentation range at tens MeV and above).

Nuclear collisions in the inner radiation zone

The data on cross sections of proton inelastic reactions with nuclei of atomic mass $A \geq 4$ were adopted from the work of Letaw *et al.* (1983) where pertinent cross sections are written as a product of atomic mass dependent and energy dependent factors, $\sigma_{\mathrm{inel}}(A,E) = \sigma(A) \cdot F(E)$ where $\sigma(A) = 45.0\mathrm{A}^{0.7} \cdot [1 + 0.016 \sin(5.3 - 2.63 \cdot \ln A)]$, mbarn, here E is a proton kinetic energy in MeV. The functional form of $F(E)$ is, $F(E) = [1 - 0.62 \cdot (\exp(-E/200)) \cdot \sin(10.9 \cdot E^{-0.28})]$. In Fig. 3 we display the resulting energy dependence of the inelastic cross sections of the p + O and p + He nuclear reactions.

For calculations of the products of nuclear reactions of protons with collisional targets of complex chemical composition, we applied a version of a nuclear reaction computer code (SHIELD) developed by Dementyev and Sobolevsky (1994). This code provides for simulation of hadron cascades in the matter. In this code, there is a transfer of nucleons, pions, kaons, antinucleons, low energy neutrons, and muons over the energy range from several MeV up to 1000 GeV, although for geophysical applications we are primarily interested in the lower energies. The ionization losses and energy straggling are fully taken into account, and the main modes of meson decay are modeled.

Hadron-nucleus interactions inside the target nucleus are comprehensively simulated on the basis of known models of nuclear reactions describing the nuclear cascade and the precompound stages of the reaction as well as evaporation/fission, multifragmentation, and Fermi break up of the residual nuclei. Each hadron cascade tree is stored completely during its simulation. The capabilities of hadron transport code depends substantially on the hadron-nucleus reaction generator used. In the SHIELD code the many stage dynamical model (MSDM) is employed for the generator. It includes known Russian nuclear reaction models. The references to these models can be found in Adeev *et al.*, (1993) and Barashenkov and Toneev (1972).

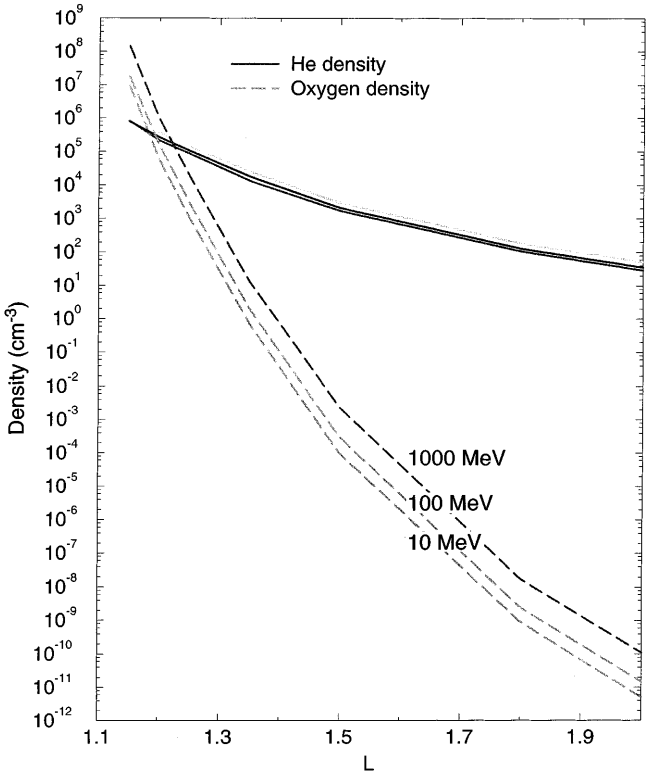

Fig. 1. The dependence on L of atmospheric He and O densities averaged over drift 10, 100, 100 MeV proton trajectory with equatorial pitch-angle of 90 degrees in the IGRF95 geomagnetic field

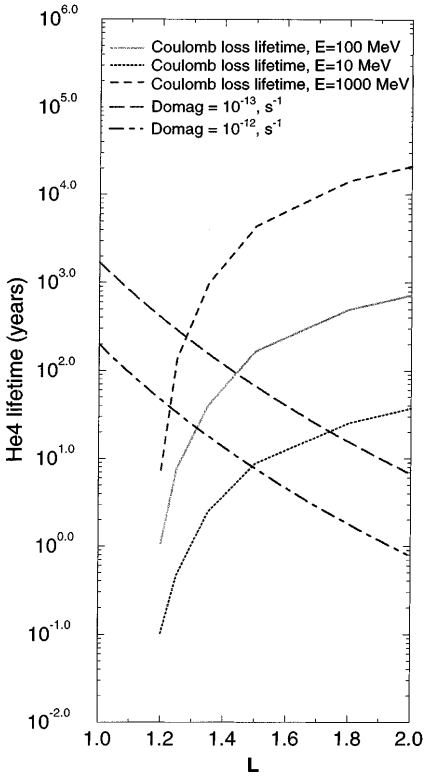

Fig. 2. Lifetime of 10–1000 MeV He ion at given L due to Coulomb energy losses and due to radial diffusion

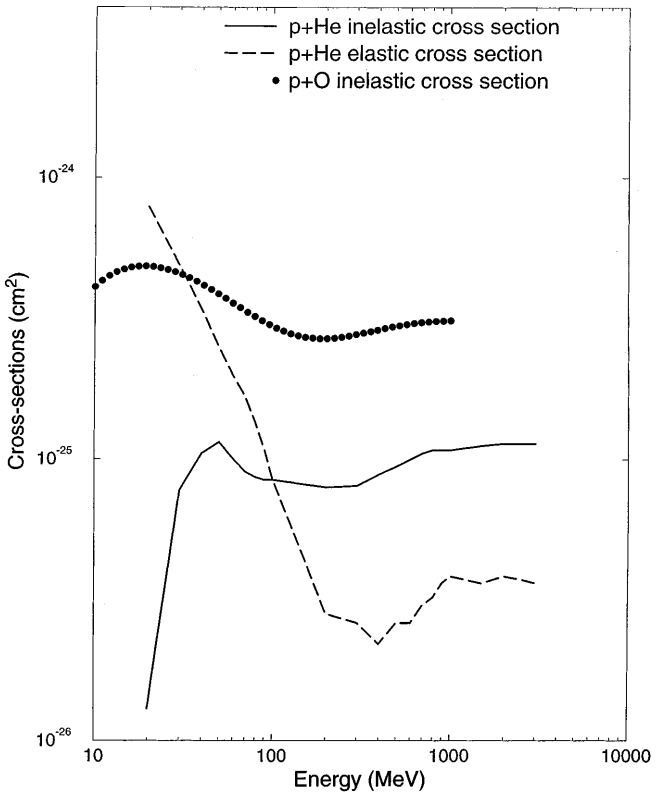

Fig. 3. Nuclear interaction cross sections versus incident proton energy for the p + O, and p + He inelastic nuclear interactions

The nuclear reaction scheme based on MSDM was first tested with a variety of experimental data about hadron-nucleus and nucleus-nucleus collisions over the range of the projectile energy: from about 15 MeV to hundreds of GeV. In the model it is assumed that the nuclear interaction process proceeds through the following subsequent stages: (1) the fast cascade stage which reduces the projectile-target interaction in a series of binary collisions between the nuclear constituents and/or produced hadrons; (2) the coalescence stage followed by the cascade in which cascade baryons can form a complex particles; (3) the stage of residual nuclei when a nucleus is becoming equilibrated (thermalized) and some particles can be emitted during this equilibration process; (4) the equilibrated de-excitation stage of nucleus which is followed by the pre-equilibrium particle emission that can be realized as a competition between Fermi decay, subsequent particle-fragment evaporation, nuclear fission or multifragmentation process.

Below we list only the nuclear models included in MSDM. More specific details of these nuclear interaction models can be found in the works of Adeev *et al.* (1993) and Barashenkov and Toneev, (1972). The fast cascade stage of reactions below 600 MeV relative kinetic energies is treated according to the Russian Dubna cascade model (Barashenkov and Toneev, 1972). Above 10 GeV the independent quark-gluon string model (QGSM) is used and in the intermediate range, 600 MeV to 10 GeV, an extension of the QGSM approach seemed an acceptable approximation. Secondary nucleons which are close in the momentum space can also form complex particles ^{2}H, ^{3}H, ^{3}He, ^{4}He according to the nuclear coalescence model. Evolution of excited residual nuclei towards the equilibrium state is described in terms of the pre-equilibrium model based on Monte Carlo solution of the corresponding master-equation.

Further equilibrium de-excitation of the residual nucleus includes several mechanisms. For light nuclei ($A < 16$) the modified Fermi break-up model is applied. Medium and heavy nuclei at moderate excitations (with nucleus energy less than 2 MeV/nucleon) suffer evaporation process including fission competition for heavy nuclei (Adeev *et al.*, 1993). Highly excited nuclei (with energy more than 2 MeV/nucleon) can decay in several excited fragments that can be described according to the statistical model of multifragmentation resulting in particles emission.

The MSDM generator code has previously been favorably applied in international benchmark calculations for comparison of results of nuclear reactions (for details, see Adeev *et al.*, 1993).

The SHIELD code provides a description of the yield of nuclear secondaries, their energy spectra and angular distributions in terms of the double differential distribution (DDD). The code uses a three-dimensional Monte Carlo simulation of the intranuclear cascade and evaporation to calculate the secondary products of the energetic proton reactions with the atmospheric constituents. The code is valid for target atomic mass $A \geq 2$.

In an application appropriate to the Earth's radiation belts, we performed Monte Carlo simulations for parent protons of energy E_p between 20 to 1000 MeV with 100 000 projectile protons and using thermal atomic oxygen and helium targets. We calculated the number of secondary D, T, ^{3}He and ^{4}He nuclei with energy, E_{sec}, between 1 to 60 MeV (with a step of 2 to 4 MeV), moving in the laboratory (i.e., the Earth-magnetosphere) system with given angle θ (ranging from 0 to 180° with a 20°) step to the velocity direction of incident parent proton.

Representative examples of the nuclear simulation outputs are given in Fig. 4 and 5. These figures give the differential energy spectra of total number D, T, ^{3}He and ^{4}He secondary nuclei (normalized to 100 000 events) of p + O reaction with E_P = 200.0 MeV (Fig. 4) and of p + He reaction with E_P = 100 MeV (Fig. 5) in the secondary particle energy range of 1 MeV up to 60 MeV.

In Fig. 6 we present an example of the resulting angle distribution of 8–10 MeV secondary ^{3}He nuclei produced in a p + He inelastic nuclear reaction with E_P = 100 MeV. The angle indicated in this figure is the angle between the secondary particle velocity vector and incident proton velocity vector.

Normalizing summary results to the number of parent protons, we obtained the DDD, describing energy and angular distributions of products of a nuclear reaction of proton with "target" nuclei, i.e. $\frac{d^2N_{sec}(E_p,E_{sec},\theta)}{dE_{sec}d\omega}$ is a number of secondary D, T and ^{3}He nuclei with energy E_{sec} and velocity direction θ, produced by one parent proton with an energy E_p in unit time, energy and in unit solid angle (here $d\omega = 2\pi\sin\theta\, d\theta$).

To evaluate a secondary nuclear product yield at various geomagnetic L-shells in the range of L = 1.1–2.0 with the L-step equal to 0.1 we integrated the product of the trapped proton differential spectrum $dN_p(E_p,L)/dE_p, \sigma_{inel}(E_p)$ and the DDD for each L-shell over the relevant proton energy range from E_p = 20 MeV to 1000 MeV:

$$\frac{d^2N_{sec}(L,E_{sec},\theta)}{dE_{sec}d\omega} = \int_{20\,MeV}^{1000\,MeV} \frac{dN_p(E_p,L)}{dE_p} \times \frac{d^2N_{sec}(E_p,E_{sec},\theta)}{dE_{sec}d\omega}\sigma_{inel}(E_p)dE_p \quad (1)$$

where $dN_p(E_p,L)/dE_p$ in protons /(cm^2 s sr keV), so that $\frac{d^2N_{sec}(E_p,E_{sec},\theta)}{dE_{sec}d\theta}$ represents a differential production spectrum i.e., a number of secondary D, T or ^{3}He nuclei with energy E_{sec} and velocity direction θ produced by the whole trapped proton spectrum at the given L-shell in unit time, in unit square, in unit secondary nucleus energy and in unit solid angle per one target nucleus. The trapped proton differential spectrum at the given L-shell was taken from AP-8 proton model (Vette, 1991).

Multiplying this spectrum by drift-averaged atmospheric densities $\bar{\rho}$ (L) for oxygen and helium we obtain

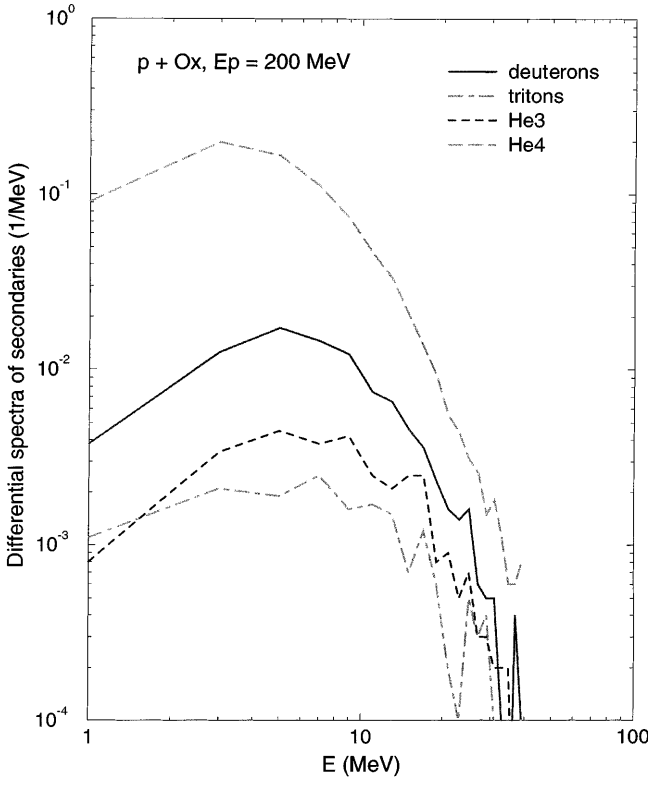

Fig. 4. The differential energy spectra of the nuclear reaction p + O products with Ep = 200.0 MeV in the total solid angle

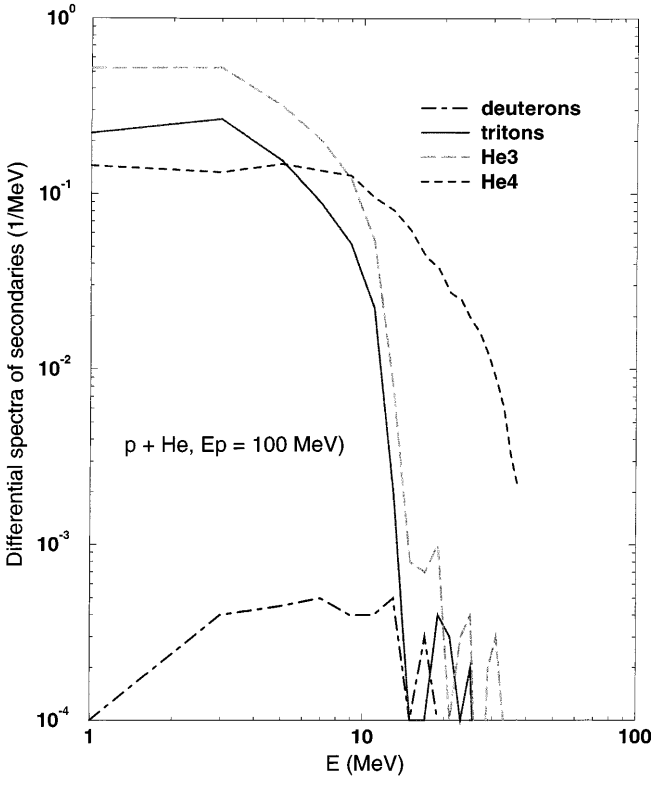

Fig. 5. The differential energy spectra of the nuclear reaction p + He products with Ep = 100.0 MeV in the total solid angle

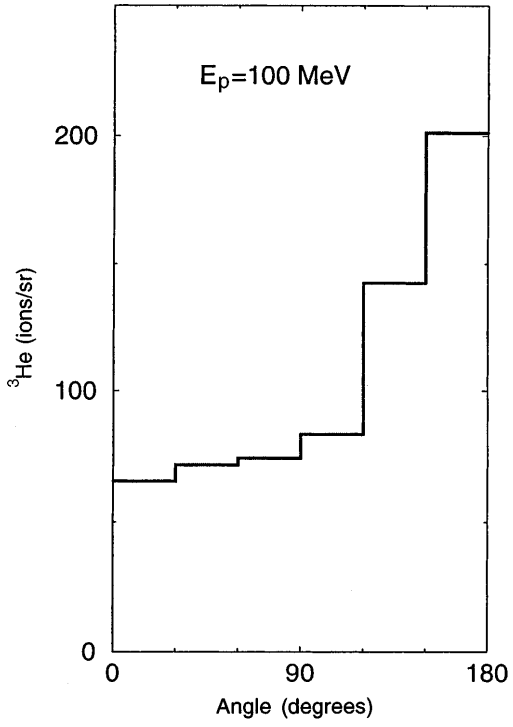

Fig. 6. An angle distribution of secondary ^{3}He nuclei with energy 8–10 MeV in the laboratory system generated by incident 100 MeV proton in the nuclear reaction p + He

an energy and angle distributions of D, T and ^{3}He nuclei generated in cm^3 by the trapped proton spectrum in nuclear reactions at a selected L-shell.

Secondary nuclei of D and ^{3}He from the p + O reaction have mainly isotropic angular distributions. This means that the nuclear evaporation products are geomagnetically trapped except the fraction that is generated within the atmospheric bounce loss cone.

In contrast to this, the products of the inelastic p + He nuclear reaction have an anisotropic angular distribution: D, T and ^{3}He secondary nuclei mostly go into the opposite hemisphere to the incident proton velocity vector (e.g., see Fig. 6). Then, considering the pitch-angle distributions of secondary nuclei, we numerically select only those secondary particles of a given energy that have velocity vector perpendicular to vector magnetic induction B, i.e., secondary particles with the pitch-angle of 90° ± 10° at the equatorial top of given L-shell. From this procedure we obtain final differential spectra of the secondary nuclei with an equatorial pitch-angle ~ 90°, $dN_{sec}(L, E_{sec})/dE_{sec}\, d\omega$ in units of ions/(cm^3 s sr keV). This result may be converted to source flux by multiplying it with the D, T, ^{3}He nuclei velocity in units of ions/cm^2 s^2 sr keV. The calculated L-shell distributions of the D, T and ^{3}He source fluxes are presented in Fig. 7 and 8.

The uncertainty involved in the source flux calculations depends on uncertainties of the cross sections, of the trapped proton fluxes, of the averaged density of MSIS model atmosphere and of the statistical errors of Monte Carlo computations. The cross sections of nuclear reactions of proton with oxygen and helium are known with a precision of about ~ 8–10% (Letaw *et al.*, 1983); trapped proton fluxes in AP-8 model are known with uncertainty of about 30–40%, and MSIS-86 atmospheric constituent densities are presented with accuracy of about 15–19% (Hedin, 1987). The statistical error of a Monte Carlo simulation is about zero at the beginning of secondary particle energy range

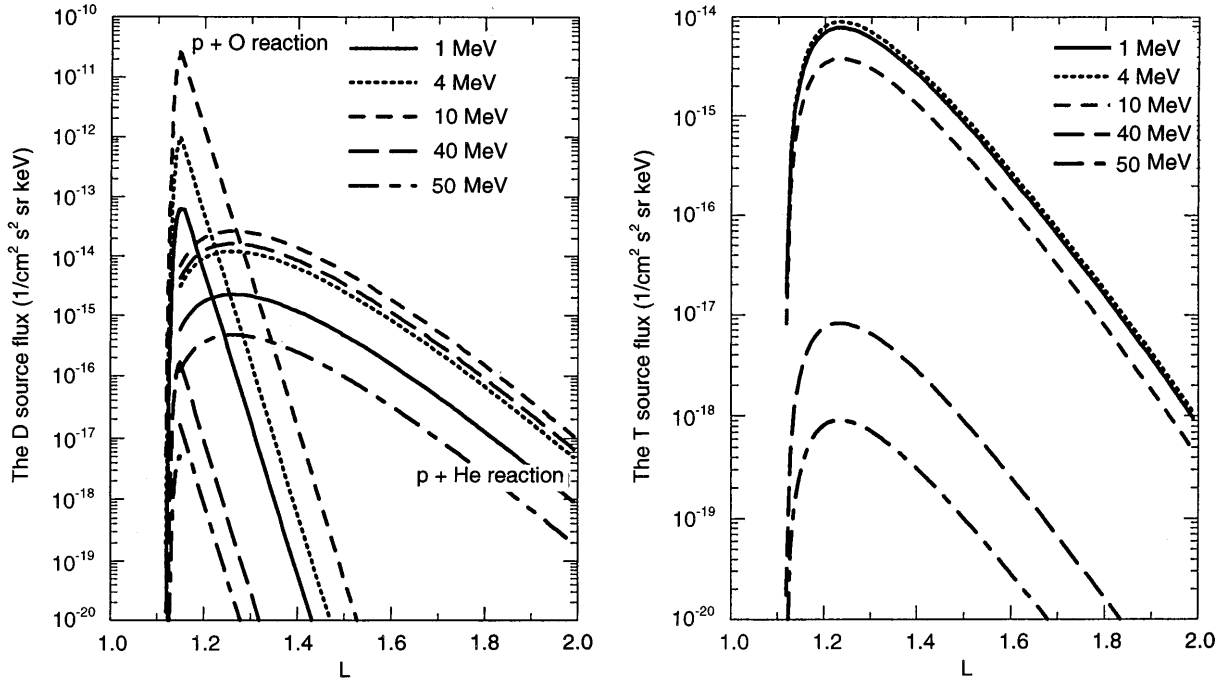

Fig. 7. Computed source fluxes of trapped D and T produced in p + O and in p + He reactions

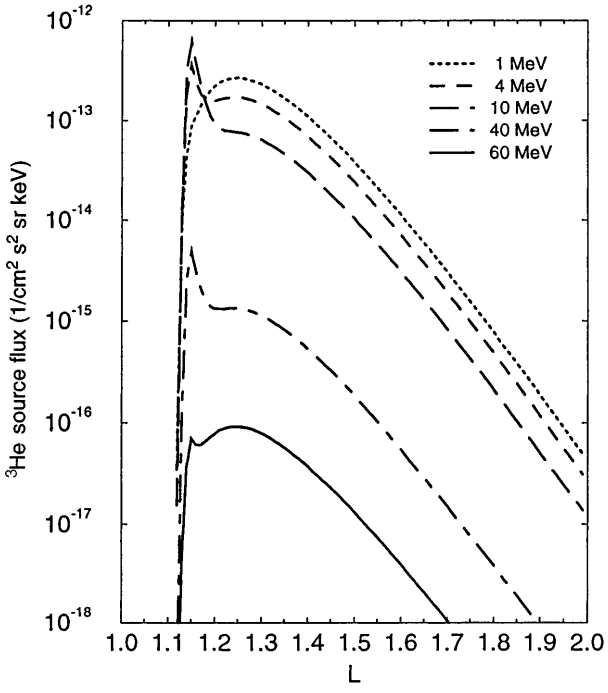

Fig. 8. Computed source fluxes of trapped ^{3}He produced in inelastic p + O and p + He reactions

($\sim$ 1 MeV), but at the end of energy range (20–30 MeV/nuc) is of about 100%. Thus, a general uncertainty of source flux is $\sim$ 50% for small energies and $\sim$ 120% for secondary nuclei of high energies.

Source, transport and loss of inner zone light isotope ions

We combined the source functions for ^{2}D and ^{3}T ions given already with radiation belt transport equations for D and T ions (e.g., Cornwall, 1972; Spjeldvik, 1997):

$$\partial f_1/\partial t = L^2\partial/\partial L[L^{-2}D_{LL_1}\partial f_1/\partial L] + S_1 + (\partial f_1/\partial t)_{\text{Coulomb}} - \Lambda_{10} f_1 \quad (2)$$

where Λ_{10} is the charge exchange frequency from singly ionized D or T ions to neutral atoms. These equations are valid for both of the hydrogen ion isotopes so long as the coefficients are calculated to pertain to the appropriate isotopic mass. For ^{3}He ions we employ the equation system (e.g., Spjeldvik, 1977):

$$\partial f_1/\partial t = L^2\partial/\partial L[L^{-2}D_{LL_1}\partial f_1/\partial L] + S_1 + (\partial f_1/\partial t)_{\text{Coulomb}} - \Lambda_{12} f_1 + \Lambda_{21} f_2 \quad (3)$$

$$\partial f_2/\partial t = L^2\partial/\partial L[L^{-2}D_{LL_2}\partial f_2/\partial L] + S_2 + (\partial f_2/\partial t)_{\text{Coulomb}} + \Lambda_{12} f_1 - \Lambda_{21} f_2 \quad (4)$$

where f_1 and f_2 are the phase space distribution functions for charge states 1+ and 2+ of ^{3}He ions, and Λ_{ij} are the charge exchange frequencies from charge state i to j.

Steady state solutions for the ambient radiation belt fluxes of these isotopic species were obtained using the finite differences technique in full implicit/fixed boundary condition form by numerical calculations (15 min of CPU time on a VAX-7610 mid-range computer). Tentatively, the ratios D/H = 1.5×10^{-4} and T/H = 3×10^{-6} ratio (by number flux) for solar cosmic rays were used to assign outer boundary conditions at outer boundary at $L = 1.6$. These ratios are not well known empirically within the radiation belts, and fortunately our results are not in significant measure dependent on these assumptions since the interior nuclear source dominates.

The radial diffusion coefficients for the Earth's radiation belts were taken from the work of Cornwall (1972) as: $D_{LL_i} = C_m L^{10} + C_e L^{10}/(L^4 + [M/(iM_o)]^2)$ as a combination of the effects of magnetic and electric fluctuations in the geomagnetic and geoelectric fields. Empirically moderate values have been chosen for the geomagnetic and geoelectric fluctuation with sub-coefficients: $C_m = 2 \times 10^{-9}$ and $C_e = 2 \times 10^{-5}$ in units of L^2 per day, and $M_o = 1$ Mev/Gauss. Over different geomagnetic activity states one might expect a variation over an order of magnitude around these values. It is also possible that fluctuating ionospheric electric fields could give rise to somewhat higher electric sub-coefficient values (Robert Sheldon, personal communication, 1990), but this is uncertain.

Figure 9a, b shows the computed radiation belt D and T ion fluxes at 1 to 60 MeV. Tritium ion fluxes were calculated here only for the p + He inelastic nuclear reaction.

From the helium isotope transport equation we compute three solutions. The first solution is with radial diffusion coefficients of $C_m = 2 \times 10^{-8}$ and $C_e = 2 \times 10^{-4}$ in units of L^2 per day, and with the moderate boundary condition ratio ^{3}He/^{4}He = 5×10^{-4} at $L = 1.6$. These results are shown in Fig. 10a. The second calculation is made with the smaller radial diffusion coefficients of $C_m = 2 \times 10^{-9}$ and $C_e = 2 \times 10^{-5}$ L^2 per day and with the same boundary condition. These results are depicted in Fig. 10b. The third illustrative set of calculations is made with transport coefficients of $C_m = 2 \times 10^{-8}$ and $C_e = 2 \times 10^{-4}$ L^2 per day and with the somewhat higher boundary condition ratio ^{3}He/^{4}He = 1×10^{-2} (Fig. 11).

Comparison of resulting ^{3}He fluxes computed with different diffusive rates (Fig. 10a, b) shows that the radial diffusion process has an influence on the flux value at $L > 1.3$–1.4 for typical ion energy above 40 MeV, and at $L > 1.4$–1.5 for less energetic ions. Certainly, this conclusion depends also on boundary flux ratio assumed here.

In Fig. 11 we see that the fluxes are determined mostly by radial diffusion process at $L > 1.3$ for ion energies more than 30 MeV and at $L > 1.4$ for smaller ion energies. But at low L-shell, i.e., at $L = 1.2$, neither the computed ^{3}He ion flux nor the deuterium ion flux (Fig. 9) are influenced significantly by radial diffusion. This demonstrates that in a narrow range of geomagnetic L-shells, internal nuclear processes within the Earth's magnetosphere dominate the generation

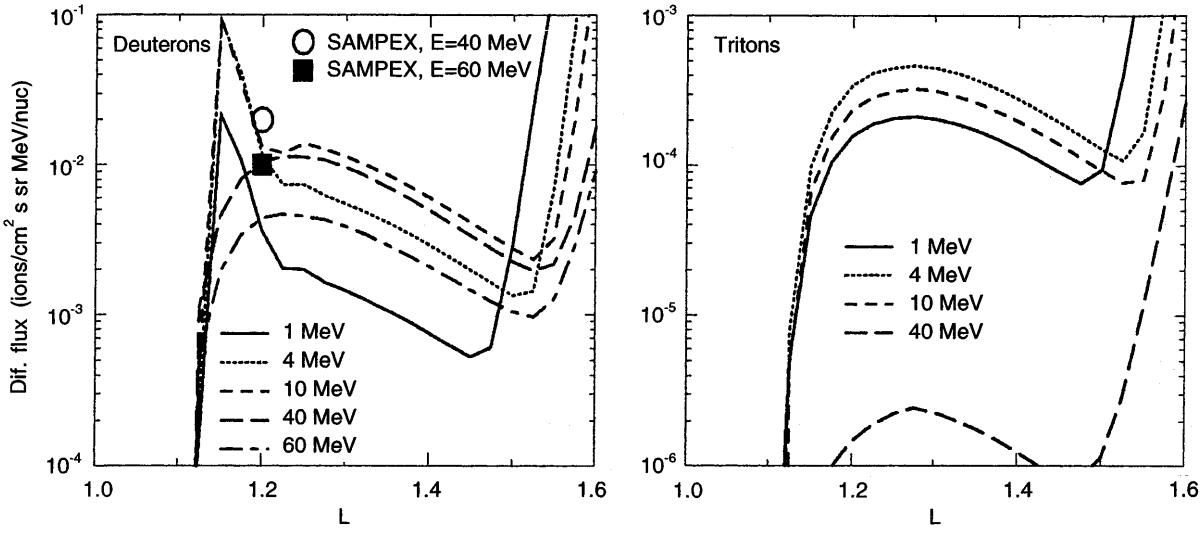

Fig. 9. Computed differential trapped *left* D and *right* T fluxes

of the lesser abundant isotopic species of the light elements.

Finally, we turn to a comparison of the results of the combined nuclear generation and geophysical transport computations with available experimental isotopic composition data obtained by the SAMPEX spacecraft team (Selesnick and Mewaldt, 1996). These researchers report energy range of the measured ions fluxes that is compatible with our calculation range. SAMPEX measurements of D flux are in the energy range of 20–60 MeV/nucleon, and ^{3}He flux measurements are in the range of 10–20 MeV/nucleon at a radiation belt location almost at the equatorial top of $L = 1.2$ and at higher invariant latitudes on other L-shells up to $L = 2.1$. In a complementary space experiment, the CRRES spacecraft helium ion isotope data are reported at higher energies, above 150 MeV. This range is, however, beyond the scope of our present computations.

Comparing the results with SAMPEX data (i.e., in Fig. 10, 11, and 12) one can see that the absolute values of the measured and computed ^{3}He fluxes agree reasonably well in the energy range of 30–60 MeV at $L = 1.2$. The computed deuterium fluxes at energies of 40 and 60 MeV at the equatorial top of $L = 1.2$ (shown in Fig. 9) are about a factor of two lower than the ones measured by SAMPEX (Selesnick and Mewaldt, 1996).

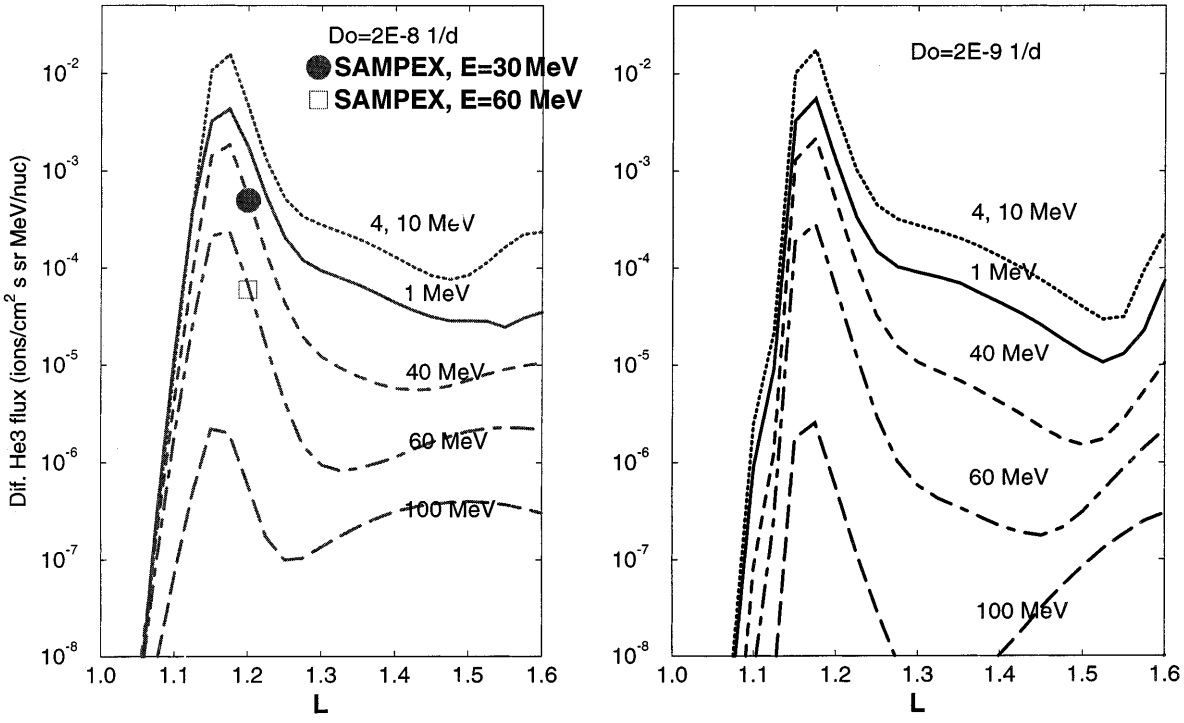

Fig. 10. Computed differential trapped ^{3}He fluxes with different radial diffusion coefficients

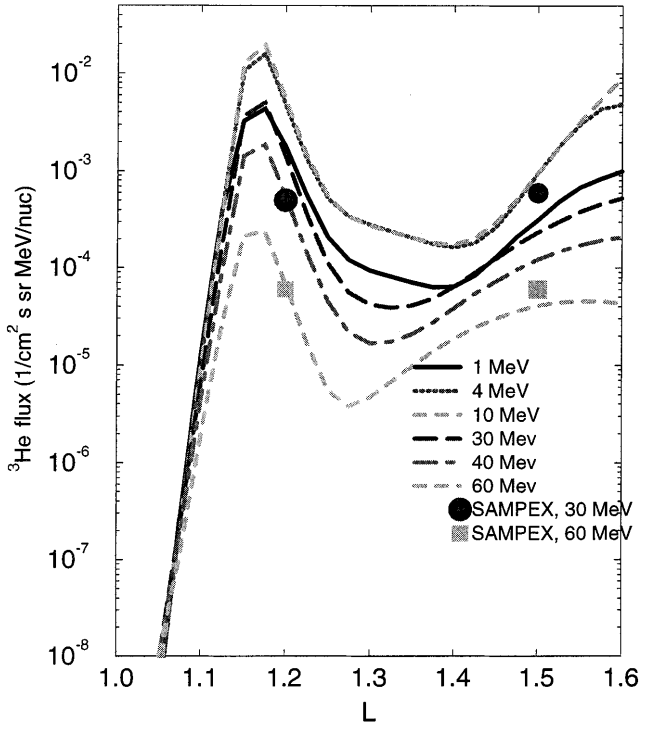

Fig. 11. Computed differential trapped ^{3}He fluxes with different boundary conditions

The authors note that the results of their own deuterium flux computations also differ by about 2–3 times from the experimentally measured deuterium ion flux. Direct comparison between theoretically predicted and measured spectra of ^{3}He flux and deuterium flux at the top of $L = 1.2$ shown in Fig. 12 also included the result of a comparison with the computed deuterium flux given by Selesnick and Mewaldt (1996). One can see that the results of measurements and computations performed by two different groups agree satisfactorily.

The computed ^{3}He fluxes at the equatorial top of $L = 1.5$ (using moderate radial diffusion rate and boundary flux ratio $^3\text{He}/^4\text{He} = 1 \times 10^{-2}$ shown in Fig. 11) are also similar to the experimental result from the SAMPEX spacecraft, although the SAMPEX results pertain to a more off-equatorial location and the comparison basis is less than ideal at that L-shell. At least, we can state that there is no glaring contradiction between our computed ^{3}He fluxes at the equatorial top of $L = 1.5$ (Fig. 11) and the measured fluxes at the foot of the same line (Selesnick and Mewaldt, 1996).

Summary and conclusion

We have computed the nuclear interaction source function of T and D and ^{3}He ions based on energetic nuclear collisions between tens of MeV radiation belt protons and minor constituents of the Earth's exosphere, thermal helium and thermal atomic oxygen. The atomic nitrogen target would also contribute to these nuclear yields, although with an efficiency of less than 10% of the yield from atomic oxygen targets. The source functions were combined with the radial diffusive transport code. It is clear that the source mechanism dominates in the region below $L = 1.2$–1.3 and produces greater fluxes of ^{3}He and of D and T than what results from inward radial diffusion alone. The L-shell where radial diffusion begins to influence on isotope flux values depends on diffusive rate and boundary (at $L = 1.6$ in our computations) flux values. Our consideration shows that radial diffusion

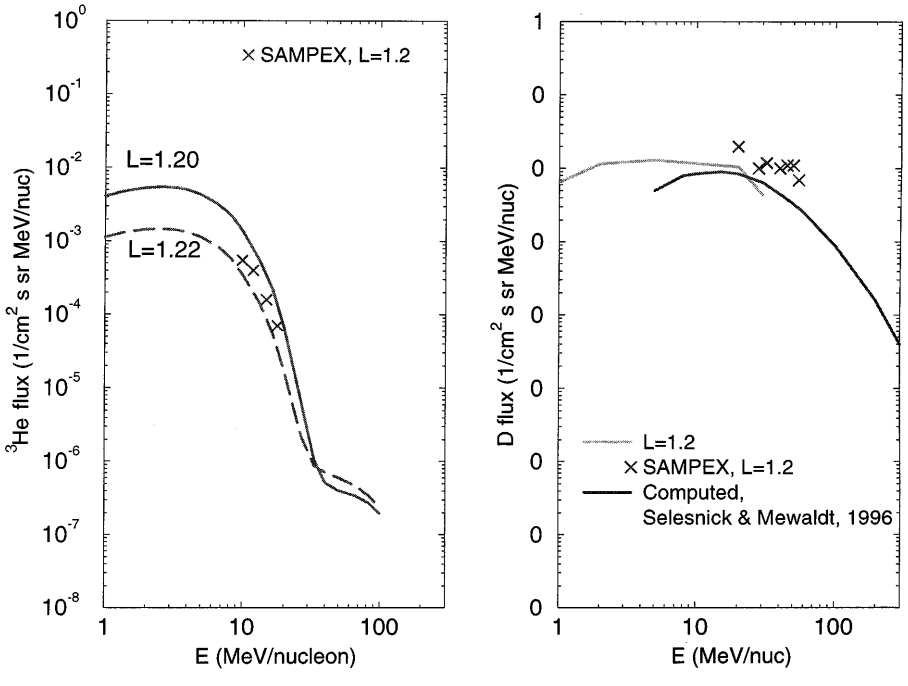

Fig. 12. Comparison of computed and measured spectra of ^{3}He and of deuterium ions at the top of $L = 1.2$

process must be taken into account at L-shells of more ~ 1.3.

To the extent that meaningful comparison between theoretical computations and space observations is possible, one can see that the computed and measured ^{3}He spectra agree quite well at the top of $L = 1.2$; the computed and measured deuterium spectra differ by a factor of two. Also, the theoretical deuterium spectra computed in this paper are similar to the deuterium results of Selesnick and Mewaldt (1996) who used a different numerical approached.

Acknowledgements. The Brazilian group was sponsored by SCTDE-SP, FAPESP-SP (93/4978-0), CNPq, FAEP of Unicamp and one of us (WNS) was sponsored in part by a NASA/GSFC research award NAS5-32915.

Topical Editor K.-H. Glassmeier thanks T. Fritz and another referee for their help in evaluating this paper.

References

Adeev, G.D., A. S. Botvina, A. S. Iljinov, and V. D. Toneev, Calculation of mass and energy distributions of fission residuals in reactions induced by intermediate energy particles. *Preprint INR*, **816/93**, Moscow, 28 pp, 1993.

Barashenkov, V.S., and V. D. Toneev, Interaction of particles and atomic nuclei of high and superhigh energies with nuclei, *Atomizdat*, Moscow, 1972.

Chen, J., T. G. Guzik, J. P. Wefel, K. R. Pyle, and J. F. Cooper, Energetic helium isotopes trapped in the magnetosphere, *J. Geophys. Res.*, **101**, 24787–24801, 1996.

Cornwall, J. M., Radial diffusion of ionized helium and protons: A probe for magnetospheric dynamics, *J. Geophys. Res.* **77** (A10), 1756–1770, 1972.

Cummings, A. C., E.C. Stone, and W. R. Webber, Distance to the solar wind termination shock and the source flux of anomalous cosmic rays during 1986–1988, *J. Geophys. Res.*, **99**, 11547–11552, 1994.

Dementyev, A. V., and N. M. Sobolevsky, SHIELD - a Monte Carlo hadron transport code, in *Proc. of Specialist's Meeting "Intermediate Energy Nuclear Data: Models and Codes"*, Paris, May 30–June 1, 1994.

Hedin, A. E., MSIS-86 thermospheric model, *J. Geophys. Res.*, **92**, 4649–4662, 1987.

Hubert F., R. Bimbot, and H. Gauvin, Ranges and stopping powers for heavy ions, *At. Data Nucl. Tables*, **46**, 1 September 1990.

Letaw, J. R., R. Silberberg, and C. H. Tsao, Proton nucleus total inelastic cross sections, an empirical formula for E > 10 MeV, *Astrophys. J. Suppl. Ser.,* **51**, 271–275, 1983.

Schulz, M., and L. J. Lanzerotti, *Particle Diffusion in the Radiation Belts*, Springer-Verlag, New York Berlin Heidelberg, 215 pp, 1974.

Selesnick, R. S., and R. A. Mewaldt, Atmospheric production of radiation belt light isotopes, *J. Geophys. Res.*, **101**, (A9), 19745–19759, 1996.

Selesnick, R. S., A. C. Cummings, J. R. Cummings, R. A. Mewaldt, E.C. Stone and T. T. von Rosenvinge, Geomagnetically trapped anomalous cosmic rays, *J. Geophys. Res.*, **100**, 9503–9518, 1995.

Spjeldvik, W. N., Equilibrium structure of equatorially mirroring radiation belt protons, *J. Geophys. Res.* **82**, 2801–2808, 1977.

Tverskoy, B. A., The Earth's radiation belts, *Science*, Moscow, Russia, 223 pp. 1968 (in Russian).

Vette, J. I., The AE-8 trapped electron model environment, *Rep. NSSDC 91-24, NASA Goddard Space Flight Center*, Greenbelt, Md., November, 1991.